RESEARCH PAPER

Comparative Investigation of Different MXene Electrodes for Enhanced Resistive Switching Performance in Solution-Processed WO_3 Memristors

Sankaraiah Guvvala[1*], Sesha Maheswaramma Kalluru[2]

[1*]Department of Chemistry, Jawaharlal Nehru Technological University Anantapur, Andhra Pradesh, India. sankarguvvala@gmail.com
[2]Department of Chemistry, Jawaharlal Nehru Technological University Anantapur College of Engineering Pulivendula, Andhra Pradesh, India.kallurumahi.chemistry@jntua.ac.in

Abstract
The tungsten oxide (WO_3) as one kind of frequently researched n-type metal oxide semiconductor possesses high electron mobility, optical transparency, chemical stability and good suitability for solution processing, which makes it a promising candidate for application in the future RRAM devices and for cost-effective and large-area electronics systems. It is worth mentioning that the electrode materials play a key role in controlling the charge injection and filament formation mechanism, and thus greatly influence the electrical characteristics and switching endurance of the WO3 based RRAM device. In the current work, we utilized the solution-processed tungsten oxide thin films as resistive switching layer, indium tin oxide (ITO) as bottom electrode and MXenes as top electrode. After coating tungsten oxide solution on ITO coated glass, thermal annealing treatment was performed to obtain the crystalline oxide films. MXene materials were deposited on the tungsten oxide film by means of spray coating. The fabricated MXene/WO_3/ITO device was found to show excellent stable bipolar resistive switching performance. The switching is chiefly determined by the formation and breaking of conductive filaments that related to oxygen vacancy migration in WO3 under applied bias, while MXene electrode with high electrical conductivity and layer structure greatly contributed to charge transportation and interface contacts. Stable resistance switching and obvious transitions between HRS and LRS have been achieved. Our finding demonstrates the potential of MXene material in solution-processed WO_3 based RRAM and might lead to novel non-volatile memory devices and Neuromorphic computing applications.

Keywords: RRAM, MXene electrodes, WO_3 thin films, ITO, resistive switching, non-volatile memory, solution-processed devices
How to cite this article: Guvvala S, Kalluru SM. Comparative Investigation of Different MXene Electrodes for Enhanced Resistive Switching Performance in Solution-Processed WO_3 Memristors. Int J Drug Deliv Technol. 2026;16(69s):485-498. DOI: 10.25258/ijddt.16.69s.55

1. Introduction

Data-centric technologies such as AI, machine learning and the internet of things are booming, creating an unprecedented demand for advanced memory systems with high speed, low energy consumption and large storage density [1]. Conventional complementary metal-oxide-semiconductor (CMOS) technology, the pillar of electronics for decades, relies on constant down-scaling of device dimensions, yet this approach encounters significant hurdles as device feature sizes approach fundamental physical limitations. Also, the traditional Von Neumann architecture separates processing from memory, leading to inefficiency and increased power consumption through frequent data transfer between the two [1],[2]. Emerging non-volatile memory technologies are under active investigation to overcome these challenges, including resistive random access memory (RRAM). RRAM's simple structure, excellent scalability and electrical performance have earned it considerable attention. These devices perform memory operations by switching between high resistance state (HRS) and low resistance state (LRS) based on the formation and rupture of conductive filaments through the dielectric layer, providing ultrafast switching, long endurance (>10^{10} cycles), high retention and scalability [2],[3]. To integrate RRAMs in large-scale circuits, crossbar arrays of memory cells are usually constructed, however this configuration requires a selector device in series with each memory cell, resulting in one-transistor-one-resistor (1T1R) configuration, which aims to eliminates neak path currents [4]. Selecting appropriate materials for switching layer and transistor is crucial for optimal RRAM performance [4]. Tungsten oxide (WO_3) is a promising material for RRAM applications owing to its superb electrical and optical properties , it is an n-type semiconductor with high electron mobility, good transparency and chemical stability. One of the main parameters governing RRAM switching behavior of WO3 based devices is the oxygen vacancies which are responsible for the formation of conductive filament as charge carriers [5],[6]. Thus by adjusting concentration of oxygen vacancies it is possible to fine-tune values of forming voltage, switching voltage, and resistance ratio [5],[6]. In addition, conventional fabrication methods such as vacuum evaporation, sputtering etc. Have limitations of high cost and difficult fabrication of large area films. Consequently, low cost solution-based techniques such as spin coating, spray coating, inkjet

*Author for Correspondence: sankarguvvala@gmail.com

printing are gaining prominence [7]. All three methods are simple, cheap, easy to perform and compatible with large-area substrates. By modifying precursor composition it is also easy to tune structural and morphological properties of the film. Tungsten oxide film fabricated by these solution based methods demonstrate excellent RRAM characteristics [7].While most work is focused on optimizing switching layer, the effect of top electrode (TE) is equally important for device performance and is responsible for injection of carriers, interface and filament formation mechanism. Conventional metals, MXenes have been extensively used as TEs , however it offers less tunability and interface instability issues [8]. Recently, MXenes are gaining interest as an emerging 2-D material for electronics applications. MXenes are a class of transition metal carbides, nitrides or carbonitrides possessing properties such as high electrical conductivity, large surface area and controllable surface chemistry. Among these materials $Ti_3C_2T_x$, V_2CT_x, Mo_2CT_x, Nb_2CT_x are promising owing to their high conductivity and strong interaction with oxide materials which is vital for them as a TEs in RRAMs [9]. In this work, WO3 based RRAM device with different MXene TEs including Ti_3C_x, V_2CT_x, Mo_2CT_x, and Nb_2CT_x is demonstrated. MXene TEs are coated using solution spray coating technique with the thickness approximately 250 nm. MXene is utilized as TE to enhance charge transport property due to high conductivity and layer structure; which results in improved interface characteristics. The use of MXene TEs significantly influences switching characteristics of RRAM devices. It depends on the type of interface formed between TE and switching layer (WO_3) and consequently may exhibit either ECM (in which metal ions migrate to form the filament) or VCM (by hopping of oxygen vacancy) and also leads to uniform filament formation [9]. Apart from that it also affects whether the switching is abrupt (essential for digital logic) or gradual (desirable for analog applications like neural computing) [10]. These properties are evaluated in terms of HRS/LRS ratio, switching voltage, endurance and retention. With an excellent performance profile, it is believed that the integration of MXene as TEs with WO_3 based RRAM devices could open novel opportunities for various applications including in-memory computing, neuromorphic devices, etc [10].

2. Experimental section

2.1. Materials

The required materials such as tungsten oxide (WO_x) (Sisco research laboratories (SRL), extra pure, 99.9%), Ethelene glycol (Honeywell, >99%), glacial acetic acid (SRL, extra pure, 99.5%), acetone (SRL, extra pure, 99%), isopropanol (SRL, pure, 99%) were procured from different sources and used in this work[11][12]. The ITO with a thickness of 180–200 nm and sheet resistance of □10 ohms sq^{-1}, coated on a glass substrate (Techinstro), was used as the bottom electrode. The UV Ozone system was procured from Revaron Pvt. Ltd and MST Manufacturing Technologies Pvt. Ltd manufactured the shadow mask. the Ti_3AlC_2,V_2AlC,Mb_2AlC,and Nb_2AlC MAX phases powder (Carbon ukraine 99.5%) Hydrochloric acid (HCl) Sigma Aldrich (99.9%), Hydrofluoric acid (HF), Lithium chloride (LiCl) TCI Pvt. Ltd[13].

2.2. Preparation of tungsten Oxide (WO_3) Solution

An aqueous solution of the tungsten oxide (WO_3) precursor was prepared using a co-solvent method in order to obtain a uniform dispersal and controllable hydrolysis. Typically, a desired amount of WO3 precursor (e.g., 0.1763 gm) was accurately weighed and put into a reaction vessel [14]. 0.8 mL ethylene glycol and 1.2 mL DI water was added to assist partial hydrolysis of the precursor in the reaction vessel. All ingredients were then mixed under constant stirring. In the next step, 100 m L glacial acetic acid was added drop-by-drop into the reaction mixture under constant stirring [15]. Acetic acid can act as a chelating agent and stabilizing agent to control the rate of hydrolysis and condensation, and is capable to obtain homogeneous solution. Then the solution was continuously stirred to form a hom_2T ogeneous and stable solution. This prepared precursor solution can be directly used for thin film deposition, coating application and the synthesis of tungsten oxide related materials.

2.3. Synthesis of MXenes

2.3.1. Synthesis of $Ti_3C_2T_x$ MXene

The $Ti_3C_2T_x$ MXene was obtained from the Ti_3AlC_2 MAX phase via top-down etching using chemical etching process and followed with exfoliation. In the etching process, Aluminum element was extracted by using mixed acid which contains hydrochloric acid and hydrofluoric acid. From the etching, a layered multilayer $Ti_3C_2T_x$ was produced with surface functional group, such as -O, -OH and -F on the surface. Wash process with neutralization then remove residual acid and byproducts from the material. As the intercalation agent to separate layered MXene, LiCl was used. It will weaken the interlayer binding force between layered MXene which separate the stacked MXene to a few layer nanosheet. And The final product was stable dispersion in water. This result proves that the $Ti_3C_2T_x$ MXene was successfully delaminated [16]. Furthermore, structural characterization results indicate that the product was indeed a MXene rather than MAX phase material. From the morphological result, it possesses the characteristic 2D layered structure and larger interlayer spacing with good stability.

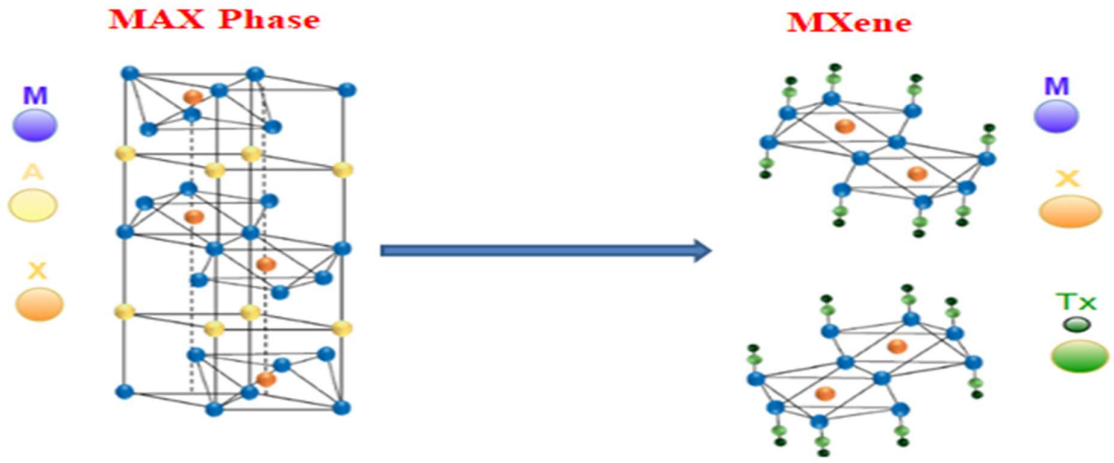

Fig.1.: Transformation mechanism of MAX phase into MXene via etching of A layer selectively. Layered MAX (in which M denotes an early transition metal element, A denote a group 13 or 14 element, and X denotes carbon and/or nitrogen) is transformed to two dimensionalMXene (MXT) by etching the A-layers to give the stacked transition metal carbide/nitride layers (T) terminated by surface functionalities (-O, -OH, -F) which increase surface energy of the materials and make them more appropriate for energy storage, catalysis, sensing, and electronics applications.

2.3.2. Synthesis of Mo_2CT_x MXene

Mo_2CTx MXene was obtained by chemical etching of the Mo_2AlC MAX phase using the LiF-HCl system, in which HF was in-situ generated. This method successfully removed the aluminum layers to form a multilayer Mo2CTx MXene with functional terminated surfaces. In this process, a relatively high reaction temperature and prolonged etching time were necessary to fully etch Al. Afterward, a repeated washing and centrifuging procedure was performed until the mixture's pH became neutral and the contaminants were removed [18][19]. Then, the stacked multilayer MXene was delaminated by using an ultrasonic treatment so that the few-layer nanosheets with a large specific surface area were obtained. As confirmed by characterizations, it has a well-formed multilayer MXene structure with increased interlayer spacing and good nanosheets' morphology. The obtained Mo_2CT_x MXene was well dispersed in aqueous solutions and showed promising characteristics [20].

2.3.3. Synthesis of V_2CT_x MXene

The V_2CT_x MXene was prepared by a chemical etching process with a fluoride chemical in V_2AlC MAX phase. Al layer was etched away with HF/HCl mixture solution with a specific condition (temperature, stirring) [21]. Multilayer V_2CT_x MXene with functional groups on the surface was fabricated through this etching process. It was washed with DI water several times to eliminate the residue chemical. The PH was near neutral after washing. The delamination was prepared with the intercalation agents and sonication method which could transform the layers into few-layered nanosheets [22]. The dispersion of MXene was stable in water because of the hydrophobic property of MXene [22].

2.3.4. Synthesis of Nb_2CT_x MXene

Nb_2CT_x MXene synthesis involved the use of a Nb_2AlC MAX phase. The bulk Nb_2AlC MAX phase was chemically etched through a top-down approach, which was then intercallated, followed by delamination. Selective etching of Al layers was carried out using HCl/HF mixed acid under heat control conditions, creating multilayer Nb_2CTx MXene covered with surface terminations like -O, -OH, -F. Washing followed after etching, via centrifugation to wash off excess acid/ by-products. The material was then intercalated, to overcome Vander waals forces to produce few layer nan sheets. This results in the formation of a stable colloid, the MXene is successfully delaminated [24,25]. Characterisation results showed that the material now has a laminated structure with expanded interlayer distances and nanoscale thicknesses.

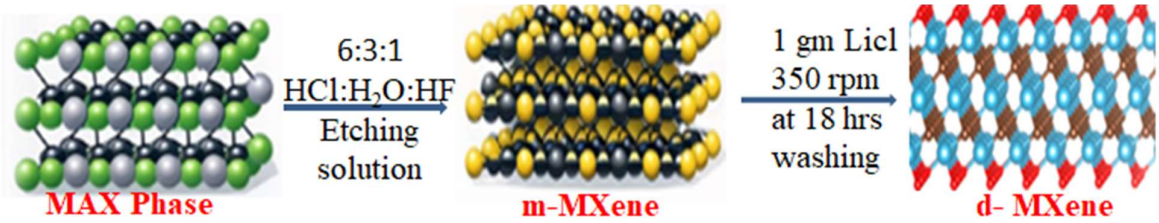

Fig.2.: Schematic representation of the synthetic method of delaminated MXene (d-MXene). 2 MAX is etched by using the mixed acidic solution of HCl:HO:HF (6:3:1) to eliminate the A-layer and formed multilayer MXene (m-MXene), then interlacing the 1 g LiCl to stir at 350 rpm for 18 h and washed by several steps, forming the few-layer or delaminated MXene (d-^{MXene}) with larger interlayer space and more surface termination groups

2.4. RRAM device fabrication

The fabrication process of the device is presented schematically in figure 1 (a). The ITO-coated glass substrates (2.3 cm X 2.3 cm) were first cleaned by sonication in DI water, acetone and isopropanol for 15 minutes. Then rinsed with isopropanol and DI water, blow-dried by the compressed air and UV-ozone treated at room temperature for 15 minutes to remove organic contaminates and improve hydrophilicity of the substrate. Then, spin coated with the solution at 3000 rpm for 30s and heated on a hot plate at 100^0C for 10 min. Deposition was carried out in 220-250^0 C and relative humidity 55-65%. Selected area etching was conducted at a corner using acetylacetone for removal of organic solvents and expose bottom contact and then anneal at 300 for 10 min in order to form the second layer as the solvent might dissolve the first deposited film. Finally, the deposited films were annealing at 400 in air for 2 hours to form the crystalline WO_3 phase (final thickness104 nm). Influence of the BE ITO device on Tungsten Oxide were deposited by DC magnetron sputtering on a two-layer WO_3/ITO. Dot architecture shadow mask with a diameter of 150 m was used for the TE deposition in order to finish the fabrication of the device. Spray-coated of TEs with diameter about 150m is the electrode where mxene like Ti_3C2T_x,V_2CT_x, Mb_2CT_x and Nb_2CT_x thicknesses were 250 nm. The thicknesses of the each TE were shown with the other elements in respectively.

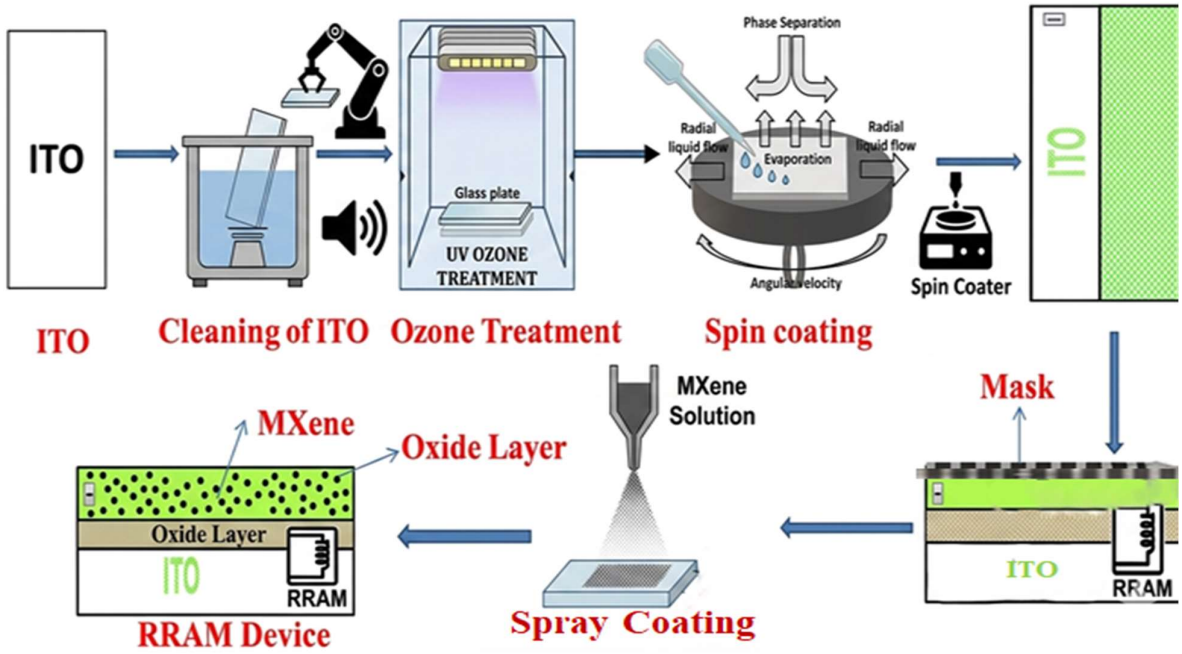

Fig.3. : Schematic workflow of the RRAM Device Architecture Design. The process involves sequential cleaning of the ITO substrate, UV-Ozone surface treatment, spin-coating of the interfacial layer, and the final deposition of the oxidized MXene active layer via spray-coating through a shadow mask.

3. Characterization of MXenes

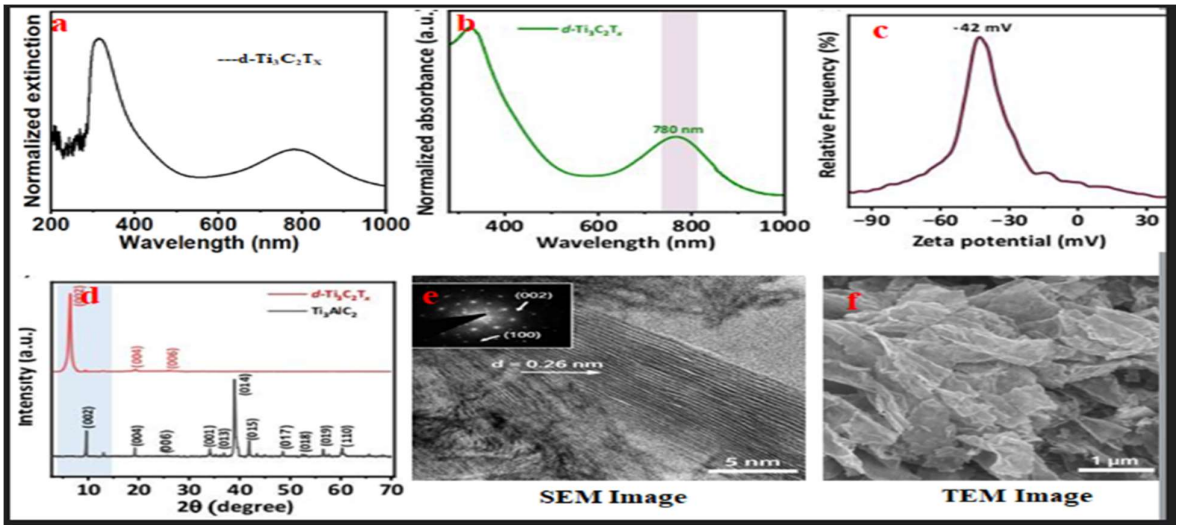

Fig.4. : The image provides a comprehensive structural and optical characterization of d-Ti3C2Tx, a specific type of two-dimensional material called a MXene. It illustrates the successful transition from a bulk ceramic to ultrathin, stable nanosheets.

Figure 4. Detailed physicochemical characterization of the delaminated $Ti_3C_2T_x$ MXene. (a,b) UV–Vis absorption spectra: Broad characteristic absorption peaks are found in the ultra violet region and the around 780 nm. These results prove the successful fabrication of $Ti_3C_2T_x$ and the existence of the metallic conductive nature owing to surface plasmon resonance. (c) Zeta potential of $Ti_3C_2T_x$ MXene: zeta potential around 42 mV indicate that the produced Ti3C2Tx MXene is highly negative and has outstanding colloidal stability in the aqueous solution. (d) XRD pattern of delaminated $Ti_3C_2T_x$ MXene. It shows the absence of characteristic peaks for the Ti_3AlC_2 MAX-phase and the strong (002) peak shifts to a smaller angle of reflection, demonstrating efficient deintercalation of Al layer and increased layer spacing of $Ti_3C_2T_x$ MXene. (e) High-resolution TEM image of $Ti_3C_2T_x$ MXene: lattice stripes with an interplanar spacing of 0.26 nm further shows the high crystallinity of the obtained nanosheets. (f)SEM image of delaminated $Ti_3C_2T_x$ MXene: An accordion-like layered morphology signifies efficient exfoliation and delamination. All these analyses suggest that high quality $Ti_3C_2T_x$ MXene materials have been successfully synthesized, which possess excellent crystallinity, high stability on the surface properties and layer structure for potential applications in various areas.

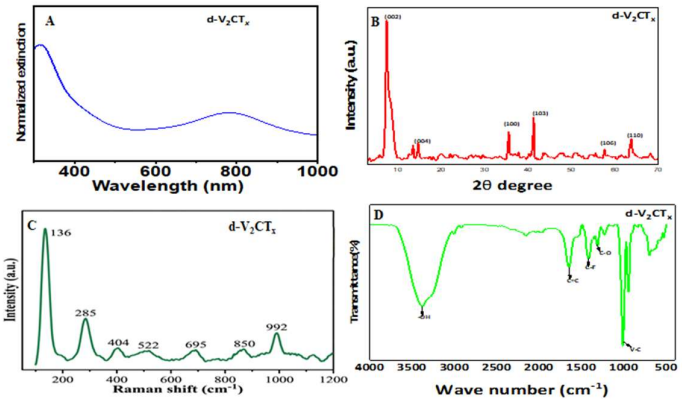

Fig.5. : Characterization of delaminated vanadium carbide MXene (d-V_2CT_x). (A) UV-Vis-NIR absorption spectrum of normalized extinction profile and large localized surface Plasmon resonance (LSPR) peak in the near-infrared area (∼790 nm). (B) XRD patterns of d-V_2CT_x shows distinctive diffraction peaks assigned to (002), (004), (100), (103), (106) and (110) crystal planes confirming delamination and phase purity. (C) Raman spectrum of d-V_2CT_x shows specific vibration modes of V-C lattice and terminations located at 136, 285, 404, 522, 695, 850 and 992 cm^{-1}. (D) FTIR spectrum of surface functional groups with specific transmission peaks for –OH (∼3400 cm^{-1}), C=C (∼1630 cm^{-1}), C-F (∼1400 cm^{-1}), C-O (∼1250 cm^{-1}) and V-C (∼1000 cm^{-1}) stretching vibration.

Figure 5 presents the optical, structural, and spectroscopic characterization of delaminated V_2CT_x MXene. The UV-Vis absorption spectrum (Fig. 5A) displays strong absorption in the UV region with a broad absorption band near 780 nm characteristic of the electronic transition and metallic feature of V_2CT_x MXene. X-ray diffraction (XRD) pattern of delaminated V_2CT_x MXene is shown in Fig. 5B.The most prominent (002) diffraction peak occurs at a low diffraction angle, which, together with other reflections (100), (101), (106) and (110), indicates that the etching process successfully removed the parent MAX phase to form high crystalline V_2CT_x with expanded interlayer spacing. Raman spectrum of delaminated V_2CT_x MXene is shown in Fig. 5C.The distinct vibrational modes are around 136, 285, 404, 522, 695, 850, and 992 cm, arising from V–C lattice vibration and surface functional groups, confirm the structural integrity and the chemical components of the prepared MXene. Fig. 5D depicts the FTIR spectrum of delaminated V2CTx MXene. The characteristic absorption peaks corresponding to -OH, C═C, C-F, C-O, and V-C groups were observed which is ascribed to numerous surface terminating groups created after etching and delamination. These functional groups increase the hydrophilicity and the chemical reactivity of MXene. These characterization data provide the successful synthesis of highly crystallized V_2CT_x MXene with rich surface termination groups and desirable optical properties, indicating promising application for energy storage, catalysis, sensing, and optoelectronic devices.

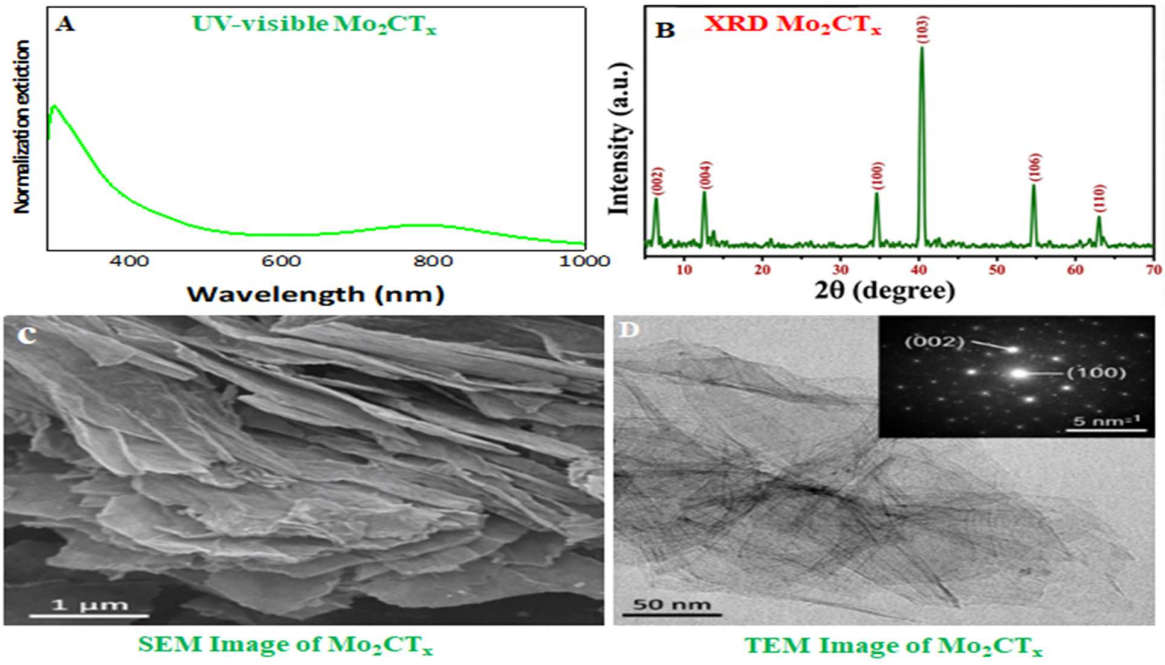

Fig.6. : Characterization of synthesized Mo_2CT_x MXene. (A) UV-visible absorption spectrum showing a primary peak at ~280 nm and a broad longitudinal surface Plasmon resonance (LSPR) peak in the 700–750 nm range. (B) XRD pattern showing the characteristic (002) and (103) diffraction planes, confirming the crystalline phase. (C) FESEM image revealing the typical multi-layered, "accordion-like" morphology. (D) TEM image of delayered Nano sheets with the inset showing the Selected Area Electron Diffraction (SAED) pattern highlighting the hexagonal symmetry of the lattice.

Figure 6 displays the optical, structural and morphological features of the prepared Mb_2CT_x MXene. The UV-Vis absorption spectra in Fig. 6A clearly shows strong absorption at ultraviolet region and a broadband absorption feature at around 780 nm, which matches the typical electronic band features and metallic properties of Mb_2CT_x MXene. The X-ray diffraction (XRD) pattern of the synthesized Mb2CTx in Fig. 6B shows a prominent peak located at 002, and other reflections around corresponding to 004, 100, 103, 106 and 110, confirming that the selective etching resulted in the crystallization of Mb_2CT_x after etching the parent MAX material. An enhanced intensity of the 002 reflection in low-angle range represents an increase of interlayer spacing, a common feature of delaminated MXene materials. From the scanning electron microscopy (SEM) image of Fig. 6C, it is observed that Mb_2CT_x MXene possesses a nice morphology featuring accordion-like stacks of nanosheets, which proves effective exfoliation of the parent materials and the retention of the two dimensional lamellar structure. In the transmission electron microscopy (TEM) image (Fig. 6D), Mb_2CT_x nanosheets is clearly ultrathin and transparent with network connection and layered assembly. In addition, the selected area electron diffraction (SAED) pattern of Mo_2CT_x MXene demonstrates clear diffraction spots (indexed as 002 and 100), which reveal its ordered structure and excellent crystallinity. Thus, the comprehensive investigations of UV-Vis absorption spectroscopy, XRD, SEM and TEM have demonstrated that well-crystallized Mb_2CT_x MXene with enlarged interlayer spacing and preserved layered morphology was successfully synthesized, showing promise in energy storage, electro catalysis, sensor and future electronic device.

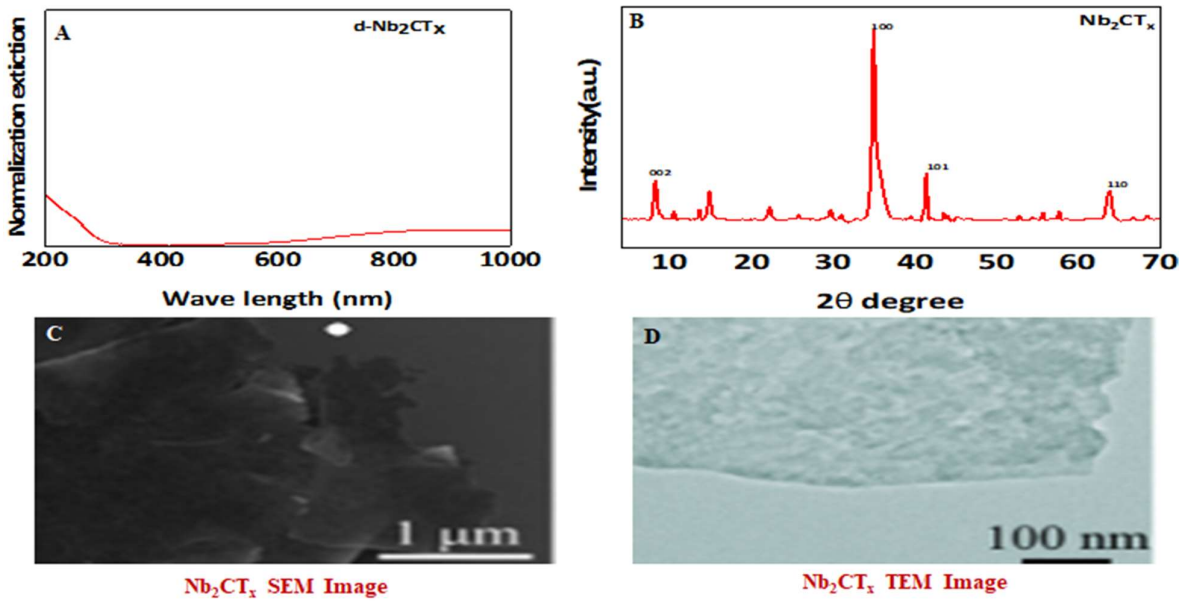

Fig.7. : Structural, optical, and morphological characterization of synthesized d- Nb_2CT_x MXene. (A) UV-Vis-NIR normalization extinction spectrum of delaminated Nb_2CT_x vs wavelength in 200-1000nm range. (B) X-ray diffraction (XRD) pattern of Nb_2CT_x, displaying the characteristic intensity peaks indexed to (002), (100), (101), and (110) crystalline planes. (C) Scanning electron microscopy (SEM) image showing the characteristic stacked layer morphology of synthesized d-Nb_2CT_x. (D) Transmission electron microscopy (TEM) image depicting the typical electron-transparent nature and thin geometry of the delaminated Nb_2CT_x nanosheet (scale bar: 100 nm).

Nb_2CT_x MXene has been synthesized and characterized structurally, optically, and morphologically, as shown in Figure 7. In terms of optical properties, as illustrated in Figure 7A, the UV-Vis absorption spectrum exhibits the characteristic absorption of the ultraviolet regime (200-300 nm) with decreasing absorption in the visible region. Such features indicate that Nb_2CT_x possesses a unique optical behaviour and could be employed in optoelectronics and related energy fields. In terms of structural, the XRD profile shown in Figure 7B clearly indicates that Nb_2CT_x is crystalline with sharp diffraction peaks located at the (002), (100), (101), and (110) crystal planes, implying the phase formation and the good crystallization of Nb_2CT_x. From the SEM image in Figure 7C, we can see the layered and accordion-like morphologies characteristic for MXenes that are achieved by etching out the MAX phases. Moreover, the resulting TEM image (Figure 7D) shows the existence of ultrathin transparent Nano sheets which maintain good layered structure as well. As a result, the good structure, morphologies, and optical characteristics confirm the formation of Nb_2CT_x MXene, promising application in advanced electronic, sensing, catalytic, and energy storage devices.

4.Electrical Switching Characteristics of Different MXene/WO_3/ITO RRAM Devices

4.1. Current–Voltage (I–V) Switching Characteristics

Resistive switching characteristics of the fabricated MXene/WO_3/ITO memory devices were examined by current-voltage (I-V) measurements under bipolar voltage sweep operation. The fabricated memory devices have different MXene electrodes as top electrode namely $Ti_3C_2T_x$, V_2CT_x, Mo_2CT_x, and Nb_2CT_x the active switching material is WO_3, the bottom electrode is ITO. It has been observed that all the fabricated devices show a clear bipolar resistive switching characteristics . During the I-V sweep both the high resistance state (HRS) and the low resistance state (LRS) are reversibly switched. The fabricated device in the initial state remained in the HRS with very small leakage current of the order of 10-6 A. Under the positive voltage sweep there was a sudden rise in the current at the SET voltage indicating the creation of conductive filament within the WO3 layer. Under negative sweep the conductive paths ruptured at the RESET voltage and switched back to HRS. This switching is non-volatile.

The $Ti_3C_2T_x/WO_3$/ITO device shows the best switching characteristics with SET voltage at about +1.5 V and ON/OFF resistance ratio is nearly 104. It is mainly due to high carrier mobility and high electrical conductivity of $Ti_3C_2T_x$ MXene which facilitates easy charge injection and better diffusion of oxygen vacancy. Slightly higher SET and RESET voltages and good stability were observed in Mo_2CT_x/WO_3/ITO device, this is because Mo_2CT_x is highly compatible at the interface of WO3. Moderate performance was seen in V_2CT_x based memory device. Nb_2CT_x electrode showed higher operating voltage owing to the relatively higher interfacial resistance.

Table 1: Electrical Switching Parameters of Different MXene/WO_3/ITO Devices

Device Structure	SET Voltage (V)	RESET Voltage (V)	ON/OFF Ratio	Switching Stability
$Ti_3C_2T_x/WO_3/ITO$	~+1.5	~−1.2	~10^4	Excellent
$Mo_2CT_x/WO_3/ITO$	~+1.7	~−1.3	~10^3	Very Good
$V_2CT_x/WO_3/ITO$	~+1.8	~−1.4	~10^3	Good
$Nb_2CT_x/WO_3/ITO$	~+2.0	~−1.5	~10^3	Moderate

From the results, we have found out that the selection of MXene electrode affects the filament formation process, charge injection efficiency and switching characteristics in a drastic way. The layer-like structure of MXene and the metallic conduction of MXenes would help in reducing the operating voltage and reliability of memory devices.

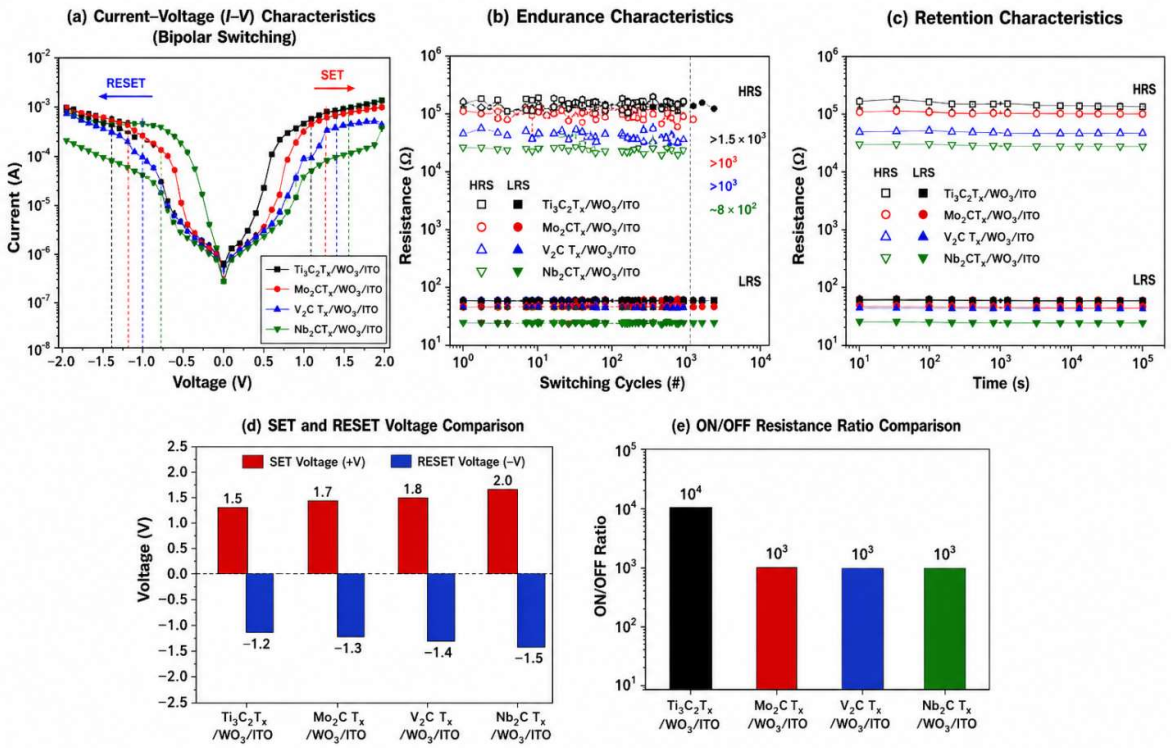

Fig 8: Electrical switching performance of MXene/WO_3/ITO RRAM devices with different MXene top electrodes. (a) I–V characteristics demonstrate stable bipolar resistive switching with distinct SET and RESET processes. (b) Endurance measurements show well-separated HRS and LRS over repeated switching cycles, indicating reliable device operation. (c) Retention characteristics confirm stable resistance states for more than 10^4 s at room temperature. (d–e) Comparison of SET/RESET voltages and ON/OFF resistance ratios reveals that the $Ti_3C_2T_x/WO_3$/ITO device exhibits the lowest operating voltage, highest ON/OFF ratio (~10^4), and the best overall memory performance among the investigated MXene electrodes.

4.2. Endurance Characteristics

Endurance is another important characteristic in characterizing the operating reliability of resistive memory devices. By repeatedly switching the memory cells between HRS and LRS under subsequent SET and RESET operations, the endurance characteristics of the devices were explored by measuring the resistance values at the read voltage of 0.1 V.

The generated MXene/WO_3/ITO memory device showed stable switching characteristic at more than 10^3 cycles; the HRS and LRS are well separated from each other throughout the endurance measurements, the value of HRS and LRS are in the range of 10^5 Ω and 10^2 Ω and the magnitude order difference of the resistance window are both around three orders of magnitude.

The best performance with small resistance variation during the cycle tested was achieved in the case of $Ti_3C_2T_x/WO_3$/ITO devices, which are ascribed to the reversible movement of oxygen vacancy within WO_3 layer and the high conductivity of $Ti_3C_2T_x$, which limit the local joule heat and avoid the destruction of filament. The Mo_2CT_x based device showed the good endurance which ascribed to the good electrochemical stability. And the small variation of the resistance for V_2CT_x and Nb_2CT_x device may due to local atomic rearrangement during frequent filament formation and rupture.

Table 2: Endurance Characteristics of MXene/WO_3/ITO Memory Devices

Device Structure	Switching Cycles	HRS (Ω)	LRS (Ω)	Stability
$Ti_3C_2T_x$/WO_3/ITO	>1.5 × 10^3	~10^5	~10^2	Excellent
Mo_2CT_x/WO_3/ITO	>10^3	~10^5	~10^2	Very Good
V_2CT_x/WO_3/ITO	>10^3	~10^5	~10^2	Good
Nb_2CT_x/WO_3/ITO	~8 × 10^2	~10^5	~10^2	Moderate

The endurance results confirm the suitability of MXene-integrated WO_3 memristors for long-term non-volatile memory applications.

4.3 Retention Characteristics

Retention is defined as the capability of memory devices to retain data over time without any power supply. Here, the retention characteristic was measured by observing resistance change of the HRS and LRS at room temperature using the read voltage 0.1 V. The three fabricated devices held the memory states constantly for longer than 10^4s. The HRS was close to 10^5 Ω and the LRS close to 10^2 Ω throughout the measuring time. There was no degradation nor overlap of memory states. All three devices exhibit good retention performance.

This stable retention characteristic is ascribed to stable conductive filaments created in WO_3 switching layer. Layered MXene electrodes promote uniform distribution of the electric field and confined confinement of oxygen vacancies which would reduce leakage of charges and the instability of the filaments. Both $Ti_3C_2T_x$ and Mo_2CT_x electrodes have the most stable retention behaviours because of stable interface with WO_3 and excellent

Table 3: Retention Performance of MXene/WO_3/ITO Devices

Device Structure	Retention Time	HRS Stability	LRS Stability
$Ti_3C_2T_x$/WO_3/ITO	>10^4 s	Stable	Stable
Mo_2CT_x/WO_3/ITO	>10^4 s	Stable	Stable
V_2CT_x/WO_3/ITO	>10^4 s	Slight fluctuation	Stable
Nb_2CT_x/WO_3/ITO	>10^4 s	Moderate stability	Stable

These results verify that MXene-based WO3 memory device exhibits superior data retention for memory applications.

4.4 Conduction Mechanism Analysis

In order to understand the charge transport process which is the driving force of resistive switching, conduction mechanism was analyzed with the logarithmic current-voltage [log(I)-log(V)] characteristic curves. From the analysis, transport mechanism were observed to have two differences in HRS and LRS.

LRS (Low Resistance State)

From [log(I)-log(V)] curve, we can find the log(I) is almost linearly proportion to log(V) with the slope of nearly one as follow:

$$I \propto V$$

Which indicating the current conduction mechanism is Ohmic. In this case, the continuous filament constructed through the aggregation of oxygen vacancy enables continuous charge transporting pathway between the MXene top electrode and ITO bottom electrode which leads to high carrier conductivity.

HRS (High Resistance State)

For HRS regions, the curve is not linearly proportional with its slope are all more than 2 as follow:

$$I \propto V^n, n>2$$

This phenomenon is a trap controlled Space Charge Limited Conduction (SCLC). In the increasing voltage, inject carriers get trapped in the defects energy states which are associated with the oxygen vacancies in WO3 layer. After these traps are progressively occupied, space-charge leads the conduction which produce this nonlinear current characteristic.

So, the switching process mechanism are based on migration of oxygen vacancy, that under positive voltage oxygen vacancy are injected to form conductive filament (SET process), and the current switched back to high resistance under reverse voltage when oxygen ions recombine with vacancies and conductive filament rupture (RESET process). MXene electrodes enhance the field concentration and charge transport rate thus resulted in low switching voltage and the consistency of device.

Table 4: Conduction Mechanism of MXene/WO_3/ITO Devices

Region	Slope	Mechanism	Physical Process
HRS (Low Voltage)	~1	Ohmic	Thermally generated carriers
HRS (High Voltage)	>2	SCLC	Trap-controlled transport
Near SET	High slope	TFL Region	Rapid trap filling
LRS	~1	Ohmic	Conductive filament

			conduction
RESET Region	>2	SCLC	Filament rupture initiation

4.5 Comparative Discussion of Different MXene Electrodes

As can be seen from the above switching performance comparisons, the choice of electrode affects the switching behaviors very much. From the experimental results, we know $Ti_3C_2T_x$ electrode shows the best performance due to high conductivity, larger surface area and good interfacial contacts between $Ti_3C_2T_x$ and WO3.The device with Mo_2CT_x electrode has good switching performance and retention performance. With V_2CT_x electrode, the devices have relatively high working voltages but good switching performance and moderate operating voltage. Nb_2CT_x device has relatively higher switching voltages due to more increased interfacial resistance and slower oxygen vacancy transfer.

1. High electrical conductivity favors better electron injection into WO_3 layer.
2. High mobility for electrons to transfer in layered 2D structures.
3. Surface functional groups of MXene (e.g., -O, -OH, -F) is helpful to increase interface quality between electrode and dielectrics.
4. Improved oxygen vacancy confinement and filament formation.
5. Low operating voltage and high cycle endurance.

These results indicate that MXene electrodes significantly improved the electrical performance of WO_3-based RRAM devices and shows a great promise for low-power and high-density non-volatile memory devices and Neuromorphic applications.

5. Discussion

It can be unambiguously concluded from the experimental results that the choice of the top electrode material is critical to determining the resistive switching performance of WO3 based RRAM devices. Though the all fabricated MXene/WO_3/ITO devices could be operated in the stable bipolar resistive switching, substantial difference in switching voltage, ON/OFF resistance ratio, endurance and retention have been observed according to the different MXene materials. The underlying factors that result in the differences mainly stem from the intrinsic conductivity, interface compatibility and the surface chemistry of the various MXene.

The performances of the devices made from various MXenes were compared and it showed that the $Ti_3C_2T_x$ based device possessed the best comprehensive performance. In addition, the relatively lower SET voltage (~1.5V), high ON/OFF resistance ratio (~10^4) and superior endurance and retention in this device indicated a more efficient formation and rupturing of conductive filament within the WO_3 switching layer. Such improvements originate from its good electrical conductivity and high carrier mobility, the quick injection of electrons and uniform distribution of oxygen vacancy migration across the WO_3 active region would happen. Furthermore, the 2D nature of the Ti3C2Tx electrode with a larger contact interface with WO3 would minimize the contact resistance and enhance field strength. Similarly, Mo_2CT_X based device had reliable switching property in terms of endurance and retention performance although operating voltage is a bit higher and OFF/ON ratio is lower compared to $Ti_3C_2T_x$.

Good stability with Mo_2CT_X and WO3 materials had contributed to form stable filament with a relatively narrow range of switching parameters and high duty cycle for repeated switching.

The V_2CT_X based device can also present bipolar switching with decent endurance, however, higher operating voltage and a lower resistance ratio were observed, potentially attributed to less efficient charge injection and much slower oxygen vacancy movement compared with the cases for Ti_3C_2Tx and Mo_2CT_X . The highest SET and RESET voltages were necessary for switching in the Nb_2CT_X based device, which may have more surface scattering and a greater charge transport obstacle resulting from more intrinsic interfaces that hinder the formation of conductive filament, thus it took larger electric energy. The logic of the mechanism analysis, conducted through the log(I)-log(V) plot, also provides further evidences.

During low-resistance state (LRS), the conduction obeys the Ohmic behaviour, which can be ascribed to conductive filaments established through the two electrodes connecting WO_3 active layer. While, during high-resistance state (HRS), a SCLC dominated by trap-assisted space-charge-limited conduction (SCLC) is observed, demonstrating the dominant role of oxygen related defects before forming well-developed filaments. Thus, this transition between the two mechanisms provides the support for the valance-change-mechanism (VCM) based resistive switching behaviour and indicates the importance of oxygen vacancy movement in determining the switching behaviours.

Taken all together, it can be concluded that the high-conductivity MXene electrodes have proved to be effective in boosting the electrical performance (low operating voltage, high resistance ratio, good endurance and retention) of solution-processed WO_3 based RRAM device, and particularly $Ti_3C_2T_x$ is the most promising as a top electrode for development of low power consumption memory devices and Neuromorphic computing systems.

6. Results

The electrical characteristics of the fabricated MXene/WO_3/ITO resistive random-access memory (RRAM) devices were characterized based on I-V, endurance, retention and conduction mechanism measurements. Four MXene materials : $Ti_3C_2T_x$, Mo_2CT_X, V_2CT_X, and Nb_2CT_X were used as top electrode in RRAM devices to study the influence of electrode materials on resistive switching behaviours. All fabricated devices showed stable bipolar resistive switching characteristics, and the solution processed

WO_3 thin film operated as an active switching layer in our RRAM device.

During first voltage sweep of all devices, there was negligible current 10^{-6} through all the devices which indicate that all devices remained in the HRS when the voltage was swept from 0 to a positive voltage and finally to a negative voltage (from -2 to 2 V in the following section) in a slow rate (0.1V/s). With a positive swept voltage applied, the current started to abruptly rise at the SET voltage due to the forming of conduct Filaments formed by drifting the oxygen vacancies through WO_3 switching layer. The application of a negative voltage causes the conductive Filaments rupture and the device restored to the HRS. The reversible transition between HRS and LRS confirms the non-volatile bipolar resistive switching operation. The results show that Ti_3C_2Tx /WO_3/ITO device has the lowest SET voltage(~1.5 V) and RESET voltage (~1.2 V) and the ON/OFF resistive ratio about 10^4 (HRS is 10^5 and LRS is 10^3).

Mo_2CT_X/WO_3/ITO device exhibits excellent switching behaviours with higher SET and RESET voltages and ON/OFF resistive ratio around 10. While V_2CT_X and Nb_2CT_X show well-established switching but the relatively higher SET and RESET voltage and lower switching uniformity resulted from larger interface resistance.

The endurance performance was investigated by cyclically applying SET/RESET sweeps for up to 10^3 cycles for each device. The endurance tests showed that all devices could sustain stable operation for more than 10^3 SET/RESET cycles with the HRS being around 10^5 and LRS being about 10^2, thereby giving an ON/OFF switching ratio of almost orders of magnitude. Ti_3C_2Tx and Mo_2CT_X devices have minimal fluctuations in resistance throughout endurance cycling and Nb_2CT_X Thus relatively larger resistance variance after several tens of SET/RESET cycling.

Room temperature retention characteristic tests show that devices maintain well separated HRS and HRS over a longer period (10^4s), signifying non-volatile switching characteristics. Ti_3C_2Tx and Mo_2CT_X showed better retention characteristics without significant changes in the HRS and HRS. Nb_2CT_X and V_2CT_X were slightly inferior to Ti_3C_2Tx and Mo_2CT_X but the influence is small on overall performance.

The conduction mechanisms of the devices in the HRS and LRS were investigated using logarithmic current-voltage (logI-logV) plots (Fig.7b). The LRS exhibits Ohm law where conduction current increases linearly with voltage (slop is close to unity), confirming metallic conduction formed by conductiv Filaments. For the HRS device, the dominant conduction mechanism could be accounted for the trap-controlled space-charge-limited conduction (SCLC) with oxygen vacancy defects States, confirming that the resistive switching is governed by the formation and rupture of oxygen vacancy conduct Filaments which leads to the Valence Change Mechanism (VCM).The experimental evidence clearly demonstrates that the performance of WO3 based RRAM strongly depends on the top electrode material. Among the four MXene electrodes utilized herein Ti3C2Tx showed promising low ON/OFF ratio of nearly 3 orders of magnitude together with excellent endurance and retention, thereby representing The most suitable candidates for non-volatile RRAM.

7. Conclusion

Solution-processed MXene/WO_3/ITO based resistive random-access memory (RRAM) devices with four types of MXene electrodes, Ti_3C_2Tx, Mo_2CT_X, Nb_2CT_X and V_2CT_X were successfully prepared and investigated for resistive switching. The prepared RRAM devices showed stable bipolar resistive switching characteristics and proved WO_3 thin films can serve as promising switching materials.

In addition, the resistive switching mechanism in the WO_3 switching layer was attributed to the formation and rupture of oxygen vacancy filament within WO_3 following the valence change mechanism (VCM).

Furthermore, the results derived from [Log(I)-Log(V)] curve indicated that the conduction mechanism for SET state was Ohmic, whereas for HRS state was trap-controlled space-charge-limited conduction (SCLC). Among them, $Ti_3C_2T_x$/ WO_3/ITO device has performed the best, offering relatively low SET voltage (around 1.5 V), high ON/OFF ratio of about 10^4, excellent endurance over 10^3 switching cycles and good retention performance of > 10^4s. This might be because the $Ti_3C_2T_x$ can offer better electrical conduction property, layer structure, favourable interface with WO_3. Mo_2CT_X electrode also possessed favourable switching performance, but for Nb_2CT_X and V_2CT_X they suffered higher operation voltages due to increased interface resistance.

In this report, the comparison of four MXene electrodes reveals their crucial influence on the switching performance of WO_3-based RRAM and highlights the potential of $Ti_3C_2T_x$ as an ideal electrode material to develop the next-generation low power consumption, high-density and stable non-volatile memories.

These insights will guide the further research and development of oxide memristor with MXene electrodes and provide a prospective strategy towards Neuromorphic, artificial intelligent and memory devices.

Acknowledgement

The authors gratefully acknowledge IIT Hyderabad for providing the necessary research facilities and financial support to carry out this study under the ANRF–PAIR programme. The authors also express their sincere thanks to Dr. Narendra Kurra and Dr. Suresh Kumar Garlapati for their valuable guidance, encouragement, and continuous support of this work.

Bibliography

1. S. Yu, “Resistive Random Access Memory (RRAM): Fundamentals and Applications,” Springer, 2022.

2. R. Waser and M. Aono, “Nanoionics-based resistive switching memories,” Nature Materials, 2022.

3. A. Chen, “A review of emerging non-volatile memory technologies,” Solid-State Electronics, 2023.

4. H.-S. P. Wong et al., “Metal–oxide RRAM,” Proceedings of the IEEE, 2022.

5. J. Robertson, “Defects and oxygen vacancies in oxide semiconductors,” Reports on Progress in Physics, 2022.

6. M. Kim et al., “WO_x-based resistive switching devices,” Applied Physics Letters, 2023.

7. S. Pawar et al., “Solution-processed WO_x memristive devices,” Journal of Materials Chemistry C, 2022.

8. B. Anasori et al., “MXenes: Synthesis and applications,” Chemical Reviews, 2023.

9. C. Zhang et al., “MXene-based resistive switching devices,” Nanotechnology, 2024.

10. T. Saini et al., “Flexible MXene-based RRAM devices,” ACS Applied Electronic Materials, 2025.

11. S. Parthiban et al., "Recent advances in tugsten oxide-based thin-film transistors for flexible electronics," IEEE Trans. Electron Devices, vol. 66, no. 1, pp. 110-120, Jan. 2019.

12. M. Ghidiu, M. R. Lukatskaya, M. Q. Zhao, Y. Gogotsi, and M. W. Barsoum, "Conductive MXene clay with high volumetric capacitance," Nature, vol. 516, no. 7529, pp. 78-81, Dec. 2014.

13. K. H. Kim et al., "Low-temperature solution-processed WO_x thin-film transistors with high performance," IEEE Electron Device Lett., vol. 32, no. 10, pp. 1385-1387, Oct. 2011.

14. B. Anasori, M. R. Lukatskaya, and Y. Gogotsi, "2D metal carbides and nitrides (MXenes) for energy storage," Nat. Rev. Mater., vol. 2, no. 1, p. 16098, Jan. 2017.

15. X. Li et al., "Resistive switching properties of In2O3 thin films synthesized by chemical solution deposition," Thin Solid Films, vol. 520, no. 2, pp. 680-684, Nov. 2011.

16. F. Shahzad et al., "Electromagnetic interference shielding with 2D transition metal carbides (MXenes)," Science, vol. 353, no. 6304, pp. 1137-1140, Sep. 2016.

17. Y. Kim et al., "Solution-processed metal oxide semiconductors for thin-film transistor applications," IEEE J. Electron Devices Soc., vol. 3, no. 3, pp. 245-251, May 2015.

18. J. Halim et al., "Synthesis and characterization of 2D molybdenum carbide (MXene)," ACS Appl. Mater. Interfaces, vol. 8, no. 45, pp. 31086-31093, Nov. 2016.

19. A. Lipatov et al., "Effect of surface functional groups on the electrical properties of Ti3C2Tx MXene," Adv. Electron. Mater., vol. 2, no. 12, p. 1600255, Dec. 2016.

20. H. Yan et al., "Recent progress in MXene-based resistive switching memory devices," J. Mater. Sci. Technol., vol. 115, pp. 165-182, Jul. 2022.

21. M. Naguib et al., "Two-dimensional transition metal carbides," ACS Nano, vol. 6, no. 2, pp. 1322-1331, Feb. 2012.

22. C. Zhang et al., "Transparent resistive random access memory based on solution-processed In2O3 films," Appl. Phys. Lett., vol. 104, no. 25, p. 253503, Jun. 2014.

23. Y. Gogotsi and B. Anasori, "The rise of MXenes," ACS Nano, vol. 13, no. 8, pp. 8491-8494, Aug. 2019.

24. Q. Xu et al., "V2CTx MXene-based flexible memristors for bionic synaptic applications," Nano Energy, vol. 67, p. 104280, Jan. 2020.

25. J. Zhou et al., "Intercalation and delamination of V2CTx MXene with LiCl for high-performance supercapacitors," Electrochim. Acta, vol. 291, pp. 222-229, Nov. 2018.

26. S. J. Kim et al., "Stable colloidal dispersions of Nb2CTx MXene in water and their application in conductive coatings," Chem. Mater., vol. 29, no. 19, pp. 8255–8262, Oct. 2017.

27. A. Khan et al., "The effect of different metal top electrodes on the performance of solution-processed indium oxide-based RRAM devices," IEEE Trans. Electron Devices, vol. 72, no. 11, pp. 4850–4857, Nov. 2025.

28. P. Dutta, S. Goswami, R. Roy, and A. K. Singh, "Spray-coated Ti3C2TX MXene electrodes for high-performance electrochromic energy storage devices," Small, vol. 21, no. 5, p. 2405371, Feb. 2025.

29. N. Pheiroijam et al., "Solution processed Ti3C2 MXene nanosheets as resistive switching layers in flexible RRAM devices for sustainable electronics," Nanotechnology, vol. 36, no. 36, p. 365201, Sep. 2025.

30. H. Yan et al., "Applications of MXenes in neuromorphic computing and memristors: From material synthesis and physical mechanisms to

integrated sensing, memory, and computation," Memristors, vol. 16, no. 1, p. 8, Feb. 2026.

31. A. Jastrzebska et al., "Biological activity and bio-sorption properties of the Ti2C studied by means of zeta potential and SEM," Int. J. Electrochem. Sci., vol. 12, pp. 2159–2172, 2017.

32. A. Arabi Shamsabadi, M. Sharifian Gh, B. Anasori, and M. Soroush, "Antimicrobial mode-of-action of colloidal Ti3C2Tx MXene nanosheets," ACS Sustain. Chem. Eng., vol. 6, no. 12, pp. 16586–16596, 2018.

33. X. Gao et al., "Titanium carbide Ti3C2Tx (MXene) enhanced PAN nanofiber membrane for air purification," J. Membr. Sci., vol. 586, pp. 162–169, 2019.

34. R. P. Pandey, K. Rasool, V. E. Madhavan, B. Aïssa, Y. Gogotsi, and K. A. Mahmoud, "Ultrahigh-flux and fouling-resistant membranes based on layered silver/MXene (Ti3C2Tx) nanosheets," J. Mater. Chem. A, vol. 6, no. 8, pp. 3522–3533, 2018.

35. C. Li et al., "The antifungal activity of graphene oxide–silver nanocomposites," Biomaterials, vol. 34, no. 15, pp. 3882–3890, 2013.

36. Y. Huang et al., "A safe and fast-charging lithium-ion battery anode using MXene supported Li3VO4," J. Mater. Chem. A, vol. 7, no. 18, pp. 11250–11256, 2019.

37. M. Alhabeb et al., "Selective etching of silicon from Ti3SiC2 (MAX) to obtain 2D titanium carbide (MXene)," Angew. Chem. Int. Ed., vol. 57, no. 19, pp. 5444–5448, 2018.

38. N. Aslfattahi et al., "Experimental investigation of energy storage properties and thermal conductivity of a novel organic phase change material/MXene as A new class of nanocomposites," J. Energy Storage, vol. 27, p. 101115, 2020.

39. S. C. Smith and D. F. Rodrigues, "Carbon-based nanomaterials for removal of chemical and biological contaminants from water: a review of mechanisms and applications," Carbon, vol. 91, pp. 122–143, 2015.

40. H. N. Nguyen, C. Chaves-Lopez, R. C. Oliveira, A. Paparella, and D. F. Rodrigues, "Cellular and metabolic approaches to investigate the effects of graphene and graphene oxide in the fungi Aspergillus flavus and Aspergillus Niger," Carbon, vol. 143, pp. 419–429, 2019.

41. X. Wang, X. Liu, J. Chen, H. Han, and Z. Yuan, "Evaluation and mechanism of antifungal effects of carbon nanomaterials in controlling plant fungal pathogen," Carbon, vol. 68, pp. 798–806, 2014.

42. M. Sawangphruk, P. Srimuk, P. Chiochan, T. Sangsri, and P. Siwayaprahm, "Synthesis and antifungal activity of reduced graphene oxide nanosheets," Carbon, vol. 50, no. 14, pp. 5156–5161, 2012.

43. A. S. Chidambaranathan, K. Mohandoss, and M. K. Balasubramaniam, "Comparative evaluation of antifungal effect of titanium, zirconium and aluminium nanoparticles coated titanium plates against C. Albicans," J. Clin. Diagn. Res., vol. 10, no. 1, pp. 56–59, 2016.

44. R. P. Allaker, "The use of nanoparticles to control oral biofilm formation," J. Dent. Res., vol. 89, no. 11, pp. 1175–1186, 2010.

45. M. Chen, H. Li, X. Wang, G. Qin, and E. Zhang, "Improvement in antibacterial properties and cytocompatibility of titanium by fluorine and oxygen dual plasma-based surface modification," Appl. Surf. Sci., vol. 463, pp. 261–274, 2019.

46. Y. Zhang et al., "Uniform self-rectifying resistive random-access memory based on an MXene-TiO2 Schottky junction," Nanoscale, vol. 14, no. 43, pp. 16168–16176, 2022.

47. R. Homsi et al., "Ti3C2Tx-MXene Based Planar Memristors on Flexible Cyclic Olefin Copolymer with Voltage-Controlled Switching Behavior for Neuromorphic Applications," Eng. Sci., vol. 38, p. 1906, 2025.

48. J. Song et al., "Low-Power Ternary Bipolar Memristor of Naturally Oxidized Porous Ti3C2Tx MXene Flakes," Small, vol. 20, no. 12, p. 2400165, 2024.

49. X. Yan et al., "MXene-Based Flexible Memory and Neuromorphic Devices: A Review on Materials and Structures," Adv. Funct. Mater., vol. 35, no. 4, p. 2410112, 2025.

50. L. Wang, S. Anwer, and B. Mohammad, "Advances on MXene-Based Memristors for Neuromorphic Computing: A Review on Synthesis, Mechanisms, and Future Directions," ACS Nano, vol. 18, no. 32, pp. 21045–21062, 2024.